

Influence of inhomogeneous broadening on the dynamics of quantum dot lasers

Original

Influence of inhomogeneous broadening on the dynamics of quantum dot lasers / Wang, C.; Gioannini, Mariangela; Montrosset, Ivo; Even, J.; Grillot, F.. - ELETTRONICO. - 9357:(2015), p. 93570L. (23rd SPIE Conference on Physics and Simulation of Optoelectronic Devices usa 2015) [10.1117/12.2079844].

Availability:

This version is available at: 11583/2645639 since: 2016-07-26T15:12:18Z

Publisher:

SPIE

Published

DOI:10.1117/12.2079844

Terms of use:

This article is made available under terms and conditions as specified in the corresponding bibliographic description in the repository

Publisher copyright

(Article begins on next page)

Influence of Inhomogeneous Broadening on the Dynamics of Quantum Dot Lasers

C. Wang^{a,b*}, M. Gioannini^c, I. Montrosset^c, J. Even^a, and F. Grillot^b

^aUniversité Européenne de Bretagne, INSA, CNRS FOTON, 20 avenue des buttes de Coesmes, 35708 Rennes Cedex 7, France

^bTelecom Paristech, Ecole Nationale Supérieure des Télécommunications, CNRS LTCI, 46 rue Barrault, 75013 Paris, France

^cDipartimento di Elettronica e Telecomunicazioni, Politecnico di Torino, 10129 Torino, Italy

* cheng.wang@insa-rennes.fr

ABSTRACT

This work theoretically studies the impacts of the inhomogeneous broadening on the modulation dynamics of quantum dot lasers using a multi-population rate equation model. The modulation dynamics shows two distinct regimes depending on the energy separation between the GS and the ES. For broadenings smaller than the GS-ES separation, the K-factor increases while the damping factor offset, the differential gain and the gain compression factor decrease with the inhomogeneous broadening. For broadenings larger than the GS-ES separation, the damping factor offset keeps almost constant while the K-factor, the differential gain and the gain compression factor increases with the inhomogeneous broadening.

Keywords: semiconductor laser, quantum dot, inhomogeneous broadening, modulation dynamics

1. INTRODUCTION

Quantum dot (QD) lasers are promising laser sources for optical fibre communications because of their attractive characteristics, such as low threshold current density [1], temperature insensitivity [2], large material gain [3] as well as high differential gain [4], [5]. However, the actual dynamical performances of QD lasers including the amplitude modulation (AM) bandwidth and the frequency chirping properties are still far away from the initial expectation, which were resulted from their unique electronic structure and the atom-like discrete states [6]. One fundamental limitation to the dynamical performances is related to the carrier populations of higher energy states such as the 3D separate confinement heterostructure barrier (SCH), 2D carrier reservoir (RS, also known as wetting layer), and the excited states (ES) inside QDs [7], [8]. Secondly, the carrier scattering rates from the non-resonant states to the lasing ground state (GS) are finite (on the order of several up to tens of picoseconds) [9]-[11], further limiting the dynamical performances [12], [13]. The last important limiting factor is the direct consequence of the growth technique. QDs are grown in a self-organized (Stranski-Krastanov) mode, leading to a near-pyramidal or truncated cone shapes [6]. The surface density of dots typically varies from 10^9 to 10^{12} dots/cm² [14]-[16]. Due to the dot size fluctuation (at least one monolayer for the QD thickness), the photoluminescence from the dot ensemble is substantially inhomogeneously broadened. The inhomogeneous broadening linewidth typically ranges from 30-80 meV at room temperature [5], [17]. It is known that the inhomogeneous broadening effect has significant impacts on the AM response as well as the linewidth enhancement factor (α -factor), which is strongly dependent on the shape of the gain spectrum [18]-[20].

This work systematically investigates the influence of inhomogeneous broadening both on the statics and dynamical properties of QD lasers, based on a set of multi-population rate equation (MPRE) model [19], [21]. The MPRE model takes into account the SCH, the RS, the first two ESs and the GS inside the dots. The broadening is incorporated by considering a Gaussian shape distribution of the dots based on the inhomogeneously broadened absorption spectrum [17]. Numerical analysis shows that the inhomogeneous broadening increases the lasing threshold, broadens the gain spectrum as well as enhances the α -factor of the GS lasing. For the small-signal AM response, the modulation bandwidth is reduced for a given bias current. Meanwhile, two featured regimes are identified depending on the energy separation

between the ES and the GS. When the inhomogeneous broadening is smaller than the ES-GS separation, the differential gain, the gain compression factor and the K-factor decrease when the broadening increases, while the K-factor increases. Once the broadening is larger than the ES-GS separation, the K-factor first drops to a low value and then increases as a function of the broadening. However, the differential gain and the gain compression factor are slightly enhanced while the damping factor offset remains almost constant.

2. RATE EQUATION MODEL

The MRPE model used in this work relies on the exciton approximation, in which the electron and the hole are treated as a neutral pair. The model takes into account the presence of the SCH barrier, the RS, two excited states (ES_2 , ES_1), and the GS. The charged carriers are firstly injected into the SCH barrier, and then transport into the RS within a time τ_{RS}^{SCH} . From the RS, carriers are captured into the ES_2 within a time τ_{ES2}^{RS} , followed by the ES_1 within a time τ_{ES1}^{ES2} . Finally, the carriers relax into the GS within a time τ_{GS}^{ES1} , where the laser emission occurs. In order to incorporate the effect of the size fluctuation of the dots, the QD ensemble is divided into N subgroups, and for each group the average energies are given by $E_{ES1,n}$, $E_{ES2,n}$, and $E_{GS,n}$, respectively ($n=1,2,\dots,N$). The occupation probability of the subgroup n in the state X ($X=ES_2, ES_1, GS$) is given by $\rho_{X,n}$. The carrier escape times from lower energy back to higher energy states are calculated following the quasi-Fermi distributions of carriers. The detailed balanced condition applied to the escape is introduced in [22]. Thus, the carrier dynamics are described by the following equations:

$$\frac{dN_{SCH}}{dt} = \frac{\eta I}{qV} - \frac{N_{SCH}}{\tau_{RS}^{SCH}} + \frac{N_{RS}}{\tau_{SCH}^{RS}} \quad (1)$$

$$\frac{dN_{RS}}{dt} = \frac{N_{SCH}}{\tau_{RS}^{SCH}} - \frac{N_{RS}}{\tau_{SCH}^{RS}} - \frac{N_{RS}}{\tau_{ES2}^{RS}} \sum_{n=1}^N (1 - \rho_{ES2,n}) G_{cv,n} + \sum_{n=1}^N \frac{N_{ES2,n}}{\tau_{RS}^{ES2}} \quad (2)$$

$$\begin{aligned} \frac{dN_{ES2,n}}{dt} = & \frac{N_{RS}}{\tau_{ES2}^{RS}} (1 - \rho_{ES2,n}) G_{cv,n} - \frac{N_{ES2,n}}{\tau_{RS}^{ES2}} - \frac{N_{ES2,n}}{\tau_{ES1}^{ES2}} (1 - \rho_{ES1,n}) + \frac{N_{ES1,n}}{\tau_{ES2,n}^{ES1}} (1 - \rho_{ES2,n}) \\ & - R_{ES2,n}^{st} - R_{ES2,n}^{Auger} - R_{ES2,n}^{sp} \end{aligned} \quad (3)$$

$$\begin{aligned} \frac{dN_{ES1,n}}{dt} = & \frac{N_{ES2,n}}{\tau_{ES1}^{ES2}} (1 - \rho_{ES1,n}) - \frac{N_{ES1,n}}{\tau_{ES2,n}^{ES1}} (1 - \rho_{ES2,n}) - \frac{N_{ES1,n}}{\tau_{GS}^{ES1}} (1 - \rho_{GS,n}) + \frac{N_{GS,n}}{\tau_{ES1,n}^{GS}} (1 - \rho_{ES1,n}) \\ & - R_{ES1,n}^{st} - R_{ES1,n}^{Auger} - R_{ES1,n}^{sp} \end{aligned} \quad (4)$$

$$\frac{dN_{GS,n}}{dt} = \frac{N_{ES1,n}}{\tau_{GS}^{ES1}} (1 - \rho_{GS,n}) - \frac{N_{GS,n}}{\tau_{ES1,n}^{GS}} (1 - \rho_{ES1,n}) - R_{GS,n}^{st} - R_{GS,n}^{Auger} - R_{GS,n}^{sp} \quad (5)$$

where $G_{cv,n}$ is the existence probability of the n th subgroup dots, which satisfies the Gaussian distribution and $\sum_{n=1}^N G_{cv,n} = 1$ [21]. The longitudinal optical modes inside the laser cavity are also grouped into M families, each one having an energy E_m . The coupled photon rate equation for the m th family is given by

$$\frac{dS_m}{dt} = \Gamma_p \nu_g S_m \sum_{n=1}^N (g_{mn}^{GS} + g_{mn}^{ES1} + g_{mn}^{ES2}) - \frac{S_m}{\tau_p} + R_m^{sp} \quad (6)$$

where the gain at mode energy E_m is given by $g(E_m) = \sum_X \sum_{n=1}^N g_{mn}^X$, with g_{mn}^X the material gain at E_m owing to the state X of the n th subgroup dot:

$$g_{mn}^{GS} = \mu_{GS} C_g N_B \frac{|P_{GS}^\sigma|^2}{E_{GS,n}} (2\rho_{GS,n} - 1) G_{cv,n} B_{cv}(E_m - E_{GS,n}) \quad (7)$$

$$g_{mn}^{ES1} = \mu_{ES1} C_g N_B \frac{|P_{GS}^\sigma|^2}{E_{ES1,n}} (2\rho_{ES1,n} - 1) G_{cv,n} B_{cv}(E_m - E_{ES1,n}) \quad (8)$$

$$g_{mn}^{ES2} = \mu_{ES2} C_g N_B \frac{|P_{ES2}^\sigma|^2}{E_{ES2,n}} (2\rho_{ES2,n} - 1) G_{cv,n} B_{cv}(E_m - E_{ES2,n}) \quad (9)$$

where $\mu_{GS} = 2$, $\mu_{ES1} = 4$, and $\mu_{ES2} = 6$ are the degeneracies including the spin of the GS, ES₁, and the ES₂. C_g is a constant as $C_g = 2\pi\hbar q^2 / (cn_r \epsilon_0 m_0^2)$ [21], N_B is the dot density per unit area, $|P_X^\sigma|^2$ is the transition matrix element of the interband recombination [19], and $B_{cv}(E_m - E_{X,n})$ is the Lorentzian homogeneous broadening function. Symbols $R_{X,n}^{Auger}$ and $R_{X,n}^{sp}$ represent the Auger and the spontaneous recombination rates of the carriers in the state X of the dot group n , respectively [22]. The stimulated recombination rate $R_{X,n}^{st}$ is:

$$R_{X,n}^{st} = \Gamma_p v_g \sum_{m=1}^M g_{mn}^X S_m \quad (10)$$

The variation of the refractive index is due to the changes of the carrier density in the dots and in the RS. The contribution from the dots (Δn_{QD}) is related to the gain change through the Kramer-Krönig relations, whereas the contribution from the RS (Δn_{RS}) originates from the plasma effect and is evaluated by the Drude model [23], [24]. Thus, the total refractive index variation $\Delta n(E_m)$ at lasing energy E_m is given by

$$\Delta n(E_m) = \Delta n_{dot}(E_m) + \Delta n_{RS}(E_m) \quad (11)$$

$$\Delta n_{dot}(E_m) = \Gamma_p \frac{\hbar c}{2E_m} C_g N_B \sum_X \sum_{n=1}^N \mu_X \frac{|P_X^\sigma|^2}{E_{X,n}} (2\rho_{X,n} - 1) G_{cv,n} D_{cv}(E_m - E_{X,n}) \quad (12)$$

$$\Delta n_{RS}(E_m) = -\frac{\Gamma_p q^2 N_{RS}}{2n_b \epsilon_0 m^* \omega_m^2} \quad (13)$$

where D_{cv} is the homogeneous broadening function of the refractive index [7], and $E_m = \hbar\omega_m$. Based on the gain and refractive index expressions, the α -factor of the laser can be finally obtained by

$$\alpha_H(E_m) = -2 \frac{\omega_m}{c} \frac{\delta[\Delta n(E_m)]}{\delta[g(E_m)]} \quad (14)$$

where the variations of the gain and the refractive index are induced by a small-step current change.

3. SIMULATION RESULTS AND DISCUSSIONS

In the simulations, all parameters of the InAs/InP Fabry-Perot QD laser under study are listed in Table I. The dots are divided into 41 subgroups, and the inhomogeneous broadening linewidth is varied from 30 meV to 80 meV. The optical modes are divided into 63-98 lines depending on the broadenings. We first investigate effects of the inhomogeneous broadenings on the steady-state properties and secondly on the dynamic characteristics.

Figure 1 shows that the threshold current is increased by almost 3 times from 6 mA to 17 mA when the broadening linewidth increases from 30 meV to 80 meV. The carrier occupation probabilities of the GS, ES₁, and ES₂ central subgroups also increase for broadening linewidth values smaller than 60 meV, while slightly decrease for broadenings larger than 60 meV. The crossover between the two regimes occurs when the broadening reaches the value of the mean energy difference between the GS and the ES₁ (56 meV as shown in Table I). Therefore, for broadenings smaller than this energy difference, only carrier populations in the GS contribute to the gain peak. For larger broadenings, not only carriers in the GS contribute to the lasing process but also those in the ES₁, hence slightly reducing the carrier occupation probability.

Table I. QD material and laser parameters used in the simulations

Symbol	Description	Value	Symbol	Description	Value
L	Active region length	8.3×10^{-2} cm	E_{ES2}	Recombination energy	0.905 eV
W	Active region width	4×10^{-4} cm	E_{ES1}	Recombination energy	0.856 eV
$R_1=R_2$	Mirror reflectivity	0.32	E_{GS}	Recombination energy	0.800 eV
n_r	Refractive index	3.5	τ_{RS}^{SCH}	Transport time	1.2 ps
α	Internal modal loss	4 cm^{-1}	τ_{ES2}^{RS}	Capture time	2.1 ps
N_B	Dot density	$7 \times 10^{10} \text{ cm}^{-2}$	τ_{ES1}^{ES2}	Relaxation time	1.2 ps
H_B	Dot height	5×10^{-7} cm	τ_{GS}^{ES1}	Relaxation time	1.2 ps
N_{layer}	QD layer number	6	T_D	Dephasing time	0.1 ps
η_i	Current injection efficiency	0.8	Γ_p	Optical confinement factor	0.06
$E_{SCH} - E_{RS}$	Energy separation	50 meV	β_{SP}	Spontaneous emission factor	1×10^{-4}
$E_{RS} - E_{ES2}$	Energy separation	40 meV	N	Dot subgroup	41
Homogeneous broadening width		5 meV	M	Photon subgroup	63-98

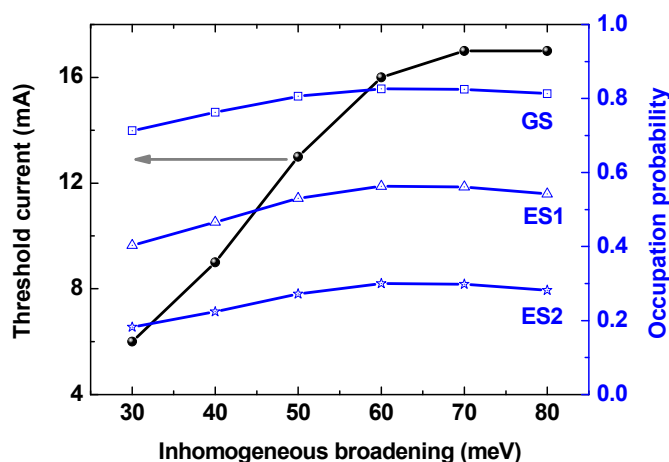


Figure 1. Variations of the laser threshold current and the carrier occupation probabilities for the QD subgroup at the center of the QD distribution (21th subgroup) as a function of the inhomogeneous broadening.

Figure 2(a) presents the net modal gain spectra at threshold based on Eqs. (7)-(9). For a broadening equal to 30 meV, the laser exhibits one narrow positive gain peak, located slightly below the average recombination energy E_{GS} of the GS. For broadening linewidth values of 40 and 50 meV, another peak appears due to the carrier population in the ES. It is noted that this peak is not located at E_{ES1} , because the peak position is determined by both the dot existence probability (Gaussian distribution) and the carrier occupation probability (Fermi distribution) for each dot subgroup. For the broadening linewidth of 60 meV, the GS and the ES_1 peaks begin to merge. For values up to 70 and 80 meV, the two peaks merge each other and form a broad gain spectrum. Carriers in the GS mainly contributes to the low-energy part of the gain, while carriers in the ES_1 contributes to the high-energy one. Following Eqs. (11)-(13), figure 2(b) shows the refractive index change $\Delta n(E_m)$ for different inhomogeneous broadenings. The index change is on the order of 10^{-4} , while the overall variation of the spectra is relatively complex. At the lasing energy E_{GS} , $\Delta n(E_{GS})$ decreases with the

increased broadenings. Figure 2(c) shows the threshold α -factor as a function of the photon energy for various inhomogeneous broadenings. Generally, the α -factor decreases with the increased photon energy. For low lasing energies, narrow inhomogeneous broadening leads to a smaller α -factor; while it is opposite for the high lasing energy case.

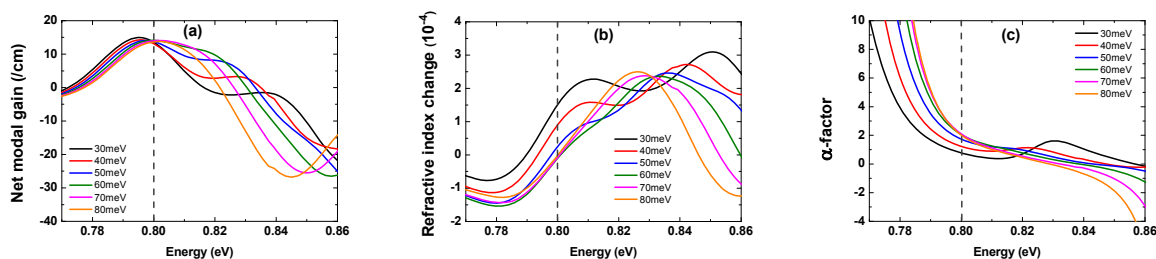


Figure 2. (a) Net modal gain ($\Gamma_p g(E_m) - \alpha_i$), (b) the refractive index ($\Delta n(E_m)$), and (c) the corresponding α -factor calculated at the lasing thresholds for various inhomogeneous broadenings. The dashed line indicates E_{GS} .

In order to obtain the AM response, we apply a step-function like current $\Delta I(t)$ (1.5 mA) to the rate equation system, then the photon response $\Delta S(t)$ is calculated in the time domain. Performing the Fourier transform to both the current and the photon responses, the AM response is obtained by $\Delta S(f) / \Delta I(f)$. Figure 3(a) shows the calculated AM responses for various inhomogeneous broadenings at a fixed bias current of 45 mA. In the first regime where the inhomogeneous broadening is smaller than the GS-ES₁ separation (56 meV), the modulation bandwidth is reduced from 4.8 GHz for broadening linewidth of 30 meV down to 2.7 GHz for 50 meV. In addition, the response is rather flat due to the strong damping of QD lasers [12]. However, in the second regime where the broadening linewidth is larger than the GS-ES₁ separation, the modulation bandwidth is slightly enhanced while the resonance peak appears in the responses. This difference is attributed to the carrier contribution of the ES, which is known to lead to a broader modulation bandwidth [19], [25]. As usually performed in experiments, we employ the well-known modulation transfer function described in [26] to fit the AM responses, in order to derive the resonance frequency f_R as well as the damping factor Γ . Figure 3(b) is a plot of the extracted damping factor as a function of the square of resonance frequency for different inhomogeneous broadenings. The studied pump currents range from near threshold up to 105 mA. Through linear fitting, the K-factor K as well as the damping factor offset Γ_0 can be extracted employing the relation $\Gamma = Kf_R^2 + \Gamma_0$ [26], and the results are shown in figure 4 as a function of the broadening linewidth.

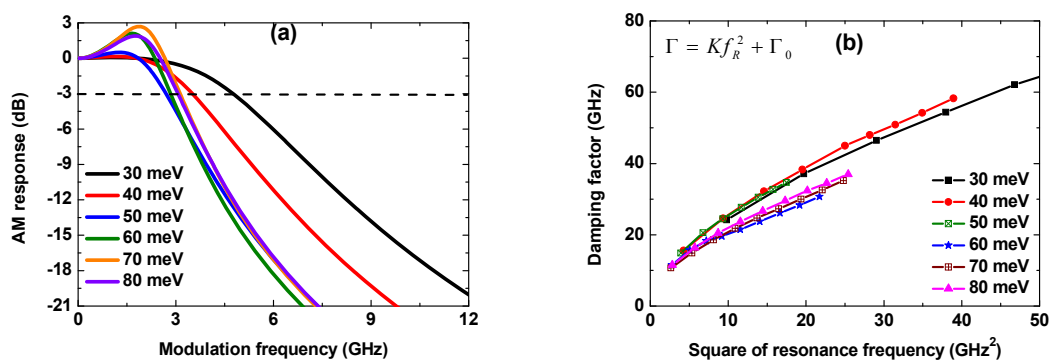


Figure 3. (a) Calculated AM response at 45 mA for the different inhomogeneous broadenings. (b) Damping factor versus the square of the resonance frequency for various bias currents.

Figure 4 reveals two different dynamical regimes separated by the mean GS-ES₁ energy separation (56 meV). The K-factor firstly increases from about 0.7 ns for a broadening linewidth of 25 meV to a maximum of 1.4 ns for 50 meV. Then, the K-factor value goes down significantly for broadening linewidths close to the GS-ES₁ separation. At the linewidth of 60 meV, the K-factor is reduced to about 0.9 ns. For larger broadening linewidths, the K-factor keeps increasing again. As for the damping factor offset, it firstly decreases with the broadening linewidth from 22.5 GHz for

linewidth of 25 meV down to about 10 GHz for 45 meV. Then, the offset value remains almost constant for broader linewidths.

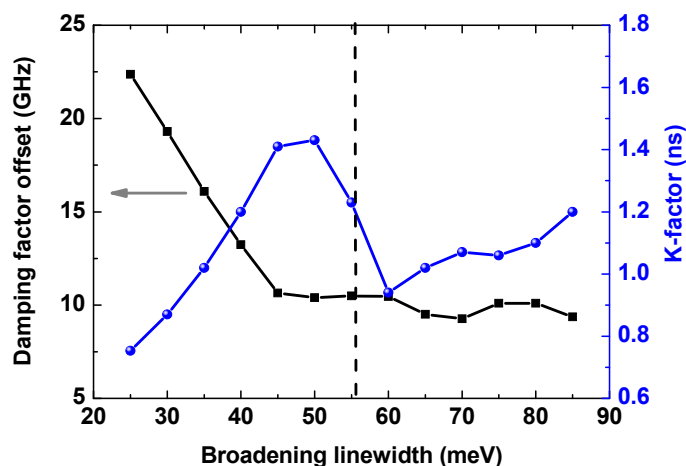


Figure 4. The calculated damping factor offset Γ_0 and the K-factor K as a function of the inhomogeneous broadening linewidth. The dashed line indicates the mean GS-ES energy separation (56 meV).

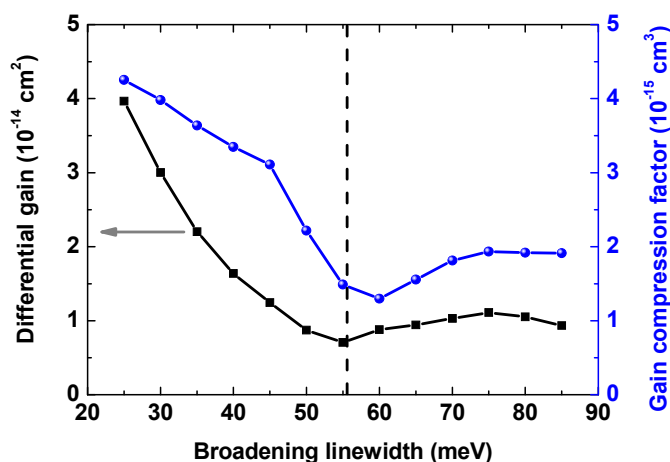


Figure 5. The calculated differential gain a and the gain compression factor ξ as a function of the inhomogeneous broadening linewidth. The dashed line indicates the mean GS-ES energy separation (56 meV).

On the other hand, through the relation between the resonance frequency and the photon density S as well as the expression of the K-factor [26] as follows, the differential gain a as well as the gain compression factor ξ can be obtained.

$$f_R^2 = \frac{v_g}{4\pi^2\tau_p} aS \quad (15)$$

$$K = 4\pi^2 \left(\tau_p + \frac{\xi}{v_g a} \right) \quad (16)$$

with τ_p the photon lifetime, and v_g the group velocity of light. Figure 5 shows the results as a function of the broadening linewidth. It is demonstrated that the behaviors also exhibit two distinct regimes. When the broadening linewidth is smaller than the mean GS-ES₁ energy separation, both the differential gain and the gain compression factor

decrease. However, on the opposite both undergo a small increase as a function of the inhomogeneous broadening linewidth in the second regime.

4. CONCLUSION

This work investigates the effects of inhomogeneous broadening on the steady-state and modulation properties of a QD laser based on a MPRE model, taking into account carrier dynamics in the SCH barrier, the RS, two ESs and the GS. Two dynamical regimes are identified. When the inhomogeneous broadening linewidth is smaller than the GS-ES energy separation, only carrier populations of the GS contribute to the lasing dynamics. The K-factor increases while the differential gain and the gain compression factor decrease with the broadening linewidth. Once the broadening linewidth is larger than the GS-ES energy separation, both carriers of the GS and the ES contribute to the modulation dynamics. The K-factor first reduces significantly and then re-increases with the broadening. In addition, the differential gain and the gain compression factor are slightly enhanced in this regime. These results give various insights on the underlying physics of QD lasers that can be exploited for the future high bandwidth and energy saving optical communication links.

ACKNOWLEDGMENTS

F. Grillot's work is supported by Partenariat Hubert Curien under Grant No. 30794RC (Campus France/DAAD). C. Wang's work is supported by China Scholarship Council.

REFERENCES

- [1] Liu, G. T., Stintz, A., Li, H., Malloy, K. J., and Lester, L. F., "Extremely low room-temperature threshold current density diode lasers using InAs dots in In Ga As quantum well," *Electron. Lett.* 35(14), 1163-1165 (1999).
- [2] Mikhlin, S. S., Kovsh, A. R., Krestnikov, I. L., Kozhukhov, A. V., Livshits, D. A., Ledentsov, N. N., Shernyakov, Y. M., Novikov, I. I., Maximov, M. V., Ustinov, V. M., and Alferov, Z. I., "High power temperature-insensitive 1.3 μ m InAs/InGaAs/GaAs quantum dot lasers," *Semicond. Sci. Technol.* 20(5), 340 (2005).
- [3] Maximov, M. V., and Ledentsov, N. N., [Quantum Dot Lasers], Dekker Encyclopedia of Nanoscience and Nanotechnology, CRC Press, 3109 (2004).
- [4] Bhattacharyya, P., Avrutin, A. A., Bryce, A. C., Marsh, J. H., Bimberg, D., Heinrichsdorff, F., Ustinov, V. M., Zaitsev, S. V., Ledentsov, N. N., Kop'ev, P. S., Alferov, Z. I., Onischenko, A. I., and O'Reilly, E. P., "Spectral and dynamic properties of InAs-GaAs self-organized quantum-dot lasers," *IEEE J. Sel. Top. Quantum Electron.* 5(3), 648-657 (1999).
- [5] Bhattacharyya, P., Klotzkin, D., Qasimeh, O., Zhou, W., Krishna, S., and Zhu, D., "High-speed modulation and switching characteristics of In(Ga)As-Al(Ga)As self-organized quantum-dot lasers," *IEEE J. Sel. Top. Quantum Electron.* 6(3), 426-438 (2000).
- [6] Bimberg, D., Grundmann, M., and Ledentsov, N. N., [Quantum Dot Heterostructures], New York Wiley, (1998).
- [7] Gioannini, M., and Montrosset, I., "Numerical analysis of the frequency chirp in quantum-dot semiconductor lasers," *IEEE J. Quantum Electron.* 43(10), 941-949 (2007).
- [8] Wang, C., Osinski, M., Even, J., and Grillot, F., "Phase-amplitude coupling characteristics in directly modulated quantum dot lasers," *Appl. Phys. Lett.* 105(22), 221114 (2014).
- [9] Siegert, J., Marcinkevicius, S., and Zhao, Q. X., "Carrier dynamics in modulation-doped InAs/GaAs quantum dots," *Phys. Rev. B* 72(8), 085316 (2005).
- [10] Uskov, A. V., Adler, F., Schweizer, H., and Pilkuhn, M. H., "Auger carrier relaxation in self-assembled quantum dots by collisions with two-dimensional carriers," *J. Appl. Phys.* 81(12), 7895-7899 (1997).
- [11] Ohnesorge, B., Albrecht, M., Oshinowo, J., Forchel, A., and Arakawa, Y., "Rapid carrier relaxation in self-assembled InxGa1-xAs/GaAs quantum dots," *Phys. Rev. B* 54(16), 11532 (1996).
- [12] Wang, C., Grillot, F., and Even, J., "Impacts of wetting layer and excited state on the modulation response of quantum-dot lasers," *IEEE J. Quantum Electron.* 48(9), 1144-1150 (2012).
- [13] Grillot, F., Wang, C., Naderi, N. A., and Even, J., "Modulation properties of self-injected quantum-dot semiconductor diode lasers," *IEEE J. Sel. Topics in Quantum Electron.* 19(4), 1900812 (2013).

- [14] Cornet, C., Schliwa, A., Even, J., Doré, F., Celebi, C., Létoublon, A., Macé, E., Paranthoën, C., Simon, A., Koenraad, P. M., Bertru, N., Bimberg, D., and Loualiche, S., "Electronic and optical properties of InAs/InP quantum dots on InP(100) and InP(311)B substrates: Theory and experiment," *Phys. Rev. B* 74(3), 035312 (2006).
- [15] Homeyer, E., Piron, R., Grillot, F., Dehaese, O., Tavernier, K., Macé, E., Le Corre, A., and Loualiche, S., "First demonstration of a 1.52 mm RT InAs/InP (311)B laser with an active zone based on a single QD layer," *Semicond. Sci. Technol.* 22(7), 827 (2007).
- [16] Kotani, J., Veldhoven, P. J., Vries, T., Smalbrugge, B., Bente, J. M., Smit, M. K., and Notzel, R., "First demonstration of single-layer InAs/InP (100) quantum-dot laser: continuous wave, room temperature, ground state," *Electron. Lett.* 45(25), 1317-1318 (2009).
- [17] Cornet, C., Labbé, C., Folliot, H., Bertru, N., Dehaese, O., Even, J., Le Corre, A., Paranthoën, C., Platz, C., and Loualiche, S., "Quantitative investigations of optical absorption in InAs/InP (311)B quantum dots emitting at 1.55 μm wavelength," *Appl. Phys. Lett.* 85(23), 5685-5687 (2004).
- [18] Dery, H., and Eisenstein, G., "The impact of energy band diagram and inhomogeneous broadening on the optical differential gain in nanostructure lasers," *IEEE J. Quantum Electron.* 41(1), 26-35 (2005).
- [19] Gioannini, M., Sevega, A., and Montrosset, I., "Simulations of differential gain and linewidth enhancement factor of quantum dot semiconductor lasers," *Optic. Quantum Electron.* 38(4-6), 381-394 (2006).
- [20] Gready, D., and Eisenstein, G., "Effects of homogeneous and Inhomogeneous broadening on the dynamics of tunneling injection quantum dot lasers," *IEEE J. Quantum Electron.* 47(7), 944-949 (2011).
- [21] M. Sugawara, K. Mukai, Y. Nakata, H. Ishikawa, and A. Sakamoto, "Effect of homogeneous broadening of optical gain on lasing spectra in self-assembled $\text{In}_x\text{Ga}_{1-x}\text{As}/\text{GaAs}$ quantum dot lasers," *Phys. Rev. B* 61(11), 7595-7603 (2000).
- [22] Grillot, F., Veselinov, K., Gioannini, M., Montrosset, I., Even, J., Piron, R., Homeyer, E., Loualiche, S., "Spectral analysis of 1.55- μm InAs/InP(113)B quantum-dot lasers based on a multi-population rate equations model," *IEEE J. Quantum Electron.* 45(7), 872-878 (2009).
- [23] Uskov, A. V., O'Reilly, E. P., McPeake, D., Ledentsov, N. N., Bimberg, D., and Huyet, G., "Carrier-induced refractive index in quantum dot structures due to transitions from discrete quantum dot levels to continuum states," *Appl. Phys. Lett.* 84(2), 272-274 (2004).
- [24] Hegarty, S. P., Corbett, B., McInerney, J. G., and Huyet, G., "Free-carrier effect on index change in 1.3 μm quantum-dot lasers," *Electron. Lett.* 41(7), 416-417 (2005).
- [25] Wang, C., Lingnau, B., Lüdge, K., Even, J., and Grillot, F., "Enhanced dynamic performance of quantum dot semiconductor lasers operating on the excited state," *IEEE J. Quantum Electron.* 50(9), 723-731 (2014).
- [26] Coldren, L. A., and Corzine, S. W., [Diode lasers and Photonic Integrated Circuits], New York Wiley, (1995).